

**Revista Mexicana de
Astronomía y Astrofísica**

Revista Mexicana de Astronomía y Astrofísica

ISSN: 0185-1101

rmaa@astroscu.unam.mx

Instituto de Astronomía

México

Garcia, Paulo; Cabrit, Sylvie; Ferreira, Jonathan; Casse, Fabien; Binette, Luc
Atomic t tauri disk winds heated by ambipolar diffusion
Revista Mexicana de Astronomía y Astrofísica, vol. 13, noviembre, 2002, pp. 21-28
Instituto de Astronomía
Distrito Federal, México

Available in: <http://www.redalyc.org/articulo.oa?id=57101306>

- How to cite
- Complete issue
- More information about this article
- Journal's homepage in redalyc.org

redalyc.org

Scientific Information System

Network of Scientific Journals from Latin America, the Caribbean, Spain and Portugal

Non-profit academic project, developed under the open access initiative

ATOMIC T TAURI DISK WINDS HEATED BY AMBIPOLAR DIFFUSION

Paulo Garcia,¹ Sylvie Cabrit,² Jonathan Ferreira,³ Fabien Casse,³ and Luc Binette⁴

RESUMEN

Resumimos resultados sobre la estructura térmica y de ionización de vientos atómicos de discos autosimilares, magnéticamente impulsados y calentados por difusión ambipolar. Mejoramos trabajos anteriores de Safier considerando (1) nuevas soluciones MHD consistentes con el equilibrio de disco kepleriano frío, (2) un tratamiento más preciso de la microfísica, y (3) predicciones para emisión de líneas espacialmente resuelta (mapas, espectros de rendija larga). La planicie de temperatura $\simeq 10^4$ K encontrada anteriormente se recupera, pero fracciones de ionización se corrigen hacia abajo por un factor de 10, por la anterior omisión de velocidades térmicas en las tasas de intercambio de momentum entre iones y neutros. Damos una idea general del origen de la planicie de temperatura. Luego comparamos las predicciones con observaciones de estrellas T Tauri, con énfasis en la necesidad de una convolución con el haz adecuado. Los anchos de los jets y las variaciones del perfil de líneas con distancias y trazadores de líneas se reproducen bien. Sin embargo, las velocidades máximas predichas son muy altas, densidades totales muy bajas y la componentes de baja velocidad [O I] es muy débil. Vientos MHD más densos y más lentos de discos tibios podrían resolver estas discrepancias.

ABSTRACT

We summarize results on the thermal and ionization structure of self-similar, magnetically-driven, atomic disk winds heated by ambipolar diffusion. We improve upon earlier work by Safier by considering (1) new MHD solutions consistent with underlying cold Keplerian disk equilibrium, (2) a more accurate treatment of the micro-physics, and (3) predictions for spatially resolved forbidden line emission (maps, long-slit spectra). The temperature plateau $\simeq 10^4$ K found earlier is recovered, but ionization fractions are revised downward by a factor of 10, due to previous omission of thermal speeds in ion-neutral momentum-exchange rates. The physical origin of the temperature plateau is outlined. Predictions are then compared with T Tauri star observations, with emphasis on the necessity of suitable beam convolution. Jet widths and variations in line profiles with distance and line tracer are well reproduced. However, predicted maximum velocities are too high, total densities too low, and the low-velocity [O I] component is too weak. Denser, slower MHD winds from warm disks might resolve these discrepancies.

Key Words: ISM: JETS AND OUTFLOWS — MAGNETOHYDRODYNAMICS — STARS: PRE-MAIN-SEQUENCE

1. INTRODUCTION

Collimated mass ejection in young T Tauri stars (TTS) is intimately correlated with the accretion process (Cohen et al. 1989; Cabrit et al. 1990; Hartigan et al. 1995; hereafter HEG95). It is currently believed that magnetic forces are responsible for both the high ejection efficiency ($\dot{M}_j/\dot{M}_{\text{acc}} \simeq 0.01\text{--}0.1$; Hartigan, Morse, & Raymond 1994, HEG95) and the high degree of collimation of these winds. Yet, the exact field structure and flow dynamics are not well established. As a result, the role played by magnetized ejection in the physics of TTS, in particular in extracting angular momentum from the circumstellar disk and/or stellar surface, remains a major enigma.

Ejection from a wide range of disk radii has been invoked to explain the compact low-velocity [O I] emission peak observed in accreting TTS (Kwan & Tademaru 1988, 1995; Hirth et al. 1994; HEG95; Kwan 1997). However, it is still unclear whether the high-velocity “microjets” observed towards several TTS could trace the outer collimated regions of the same disk wind, or whether they require a distinct ejection component.

A new tool to discriminate between models consists in confronting theoretical predictions with recent *spatially resolved* observations of the inner wind structure of TTS in optically thin forbidden lines of [O I], [S II], and [N II] (see the contributions to this volume: Bacciotti 2002; Dougados, Cabrit, & Lavalley-Fouquet 2002; Ray & Mundt 2002, and refs. therein).

Of the wide variety of models available in the literature, only two classes have self-consistent sta-

¹Centro de Astrofísica da UP, Portugal & CRAL, France

²Observatoire de Paris, DEMIRM, France

³Laboratoire d’Astrophysique, Obs. de Grenoble, France

⁴Instituto de Astronomía, UNAM, México

tionary MHD solutions that have been used for detailed observational predictions: (1) *disk winds* from a wide range of disk radii (Blandford & Payne 1982; Ferreira 1997) and (2) *X-winds* from a tiny region of open stellar field lines near the disk corotation radius (Shu et al. 1995). Both are in the regime of “cold” MHD, where ejection is only possible by magneto-centrifugal launching on field lines sufficiently inclined from the disk axis, as thermal energy is insufficient to cross the potential barrier (unlike in the solar wind).

Synthetic maps and long-slit spectra were first presented by Shang, Shu, & Glassgold (1998) and Cabrit et al. (1999) for X-winds and disk winds respectively, using a parametrized temperature and ionization fraction. More reliable predictions require actually solving for the wind thermal and ionization state, given some local heating mechanism. Shock heating was recently invoked to explain line ratios in the outer regions of microjets (Dougados et al., Lavalley-Fouquet et al. 2000) but this mechanism is not fully consistent with a stationary solution and involves additional free parameters. Other modes of mechanical energy dissipation (e.g., turbulence) have the same drawbacks.

Here, we consider only a heating process intrinsic to MHD winds of low ionization, namely ion-neutral frictional drag (*ambipolar diffusion heating*), which was first applied to predict integrated forbidden line emission in disk winds by Safier (1993a,b). It requires no extra free parameter and is self-consistently determined by the disk wind MHD structure. It will yield the “minimum” possible emission fluxes and ionization level, but emission maps and line profiles should still provide useful tests of the model collimation and dynamics. A detailed account of our results is given in Garcia et al. (2001a,b).

2. THERMAL AND IONIZATION STRUCTURE

2.1. Method and Improvements Over Previous Work

We follow the same general approach as in the pioneering work by Safier (1993a). We follow a fluid cell along a given flow streamline, characterized by ϖ_0 , the field line footpoint radius in the disk midplane, and solve for its coupled temperature and ionization evolution, including all relevant heating and cooling terms. We check a posteriori that the single, cold fluid assumptions made in computing the dynamical MHD solution remain valid, i.e., that drift speeds between ions and neutrals are small compared to the bulk flow speed, and that thermal pressure gradients are negligible compared to other forces. Our equations, heating/cooling terms, and

self-consistency checks are described in Garcia et al. (2001a). Important improvements to the work of Safier (1993a) include:

- (i) Use of new self-similar cold disk wind solutions from Ferreira (1997), where vertical equilibrium of the Keplerian accretion disk is treated self-consistently. The mass loading and magnetic lever arm are then fixed by a single parameter: the ejection efficiency in the disk, $\xi = d \ln \dot{M}_{\text{acc}} / d \ln \varpi_0$.
- (ii) Treatment of the ionization evolution of heavy elements (C, N, O, S, Ca, Mg, Fe, ...), photoionization heating, and cooling by hydrogen recombination lines, using the MAPPINGS Ic code (Binette et al. 1985, Binette & Robinson 1987).
- (iii) Correct computation of ion-neutral momentum exchange rates for ambipolar diffusion, including thermal speeds (cf. Draine 1980).
- (iv) Depletion of heavy atoms onto grains outside the dust sublimation cavity (Savage & Sembach 1996).

2.2. MHD Solution Parameters

To limit the number of free parameters, we fix the disk aspect ratio $\varepsilon = h/r = 0.1$, as indicated by observations of HH 30 (Burrows et al. 1996), and set the magnetic turbulence level parameter (controlling disk accretion across field lines) to $\alpha_m = 1$ (cf. Ferreira 1997). The central star mass is taken as $0.5 M_\odot$. Thus only 2 free global parameters are left:

- (1) The ejection efficiency parameter ξ , which typically ranges between 0.005 and 0.01 for the above ε and α_m . Our disk wind extends from ϖ_i to $10 \times \varpi_i$ and thus $\xi \sim \dot{M}_{\text{jet}}/\dot{M}_{\text{acc}}$ as observed in TTS.
- (2) The disk accretion rate, \dot{M}_{acc} , which determines both the jet density scalings and the photoionizing UV flux from the accretion disk boundary layer. We consider values between 10^{-8} and $10^{-5} M_\odot \text{ yr}^{-1}$, covering the observed range in accreting TTS (HEG95).

2.3. Results

Figure 1 presents the computed temperature, electronic density n_e , and proton fraction f_p along two streamlines for a typical solution with an intermediate ξ value of 0.007 and various mass accretion rates. The main results are the following:

- The temperature reaches a plateau around 10^4 K over most of the jet extent for the range of parameters applicable to T Tauri disk winds.
- The proton fraction f_p rises steeply at the wind base, then freezes out in the far jet region ($\chi = z/\varpi_0 \geq 300$) where densities are low and ionization timescales exceed dynamical timescales. In

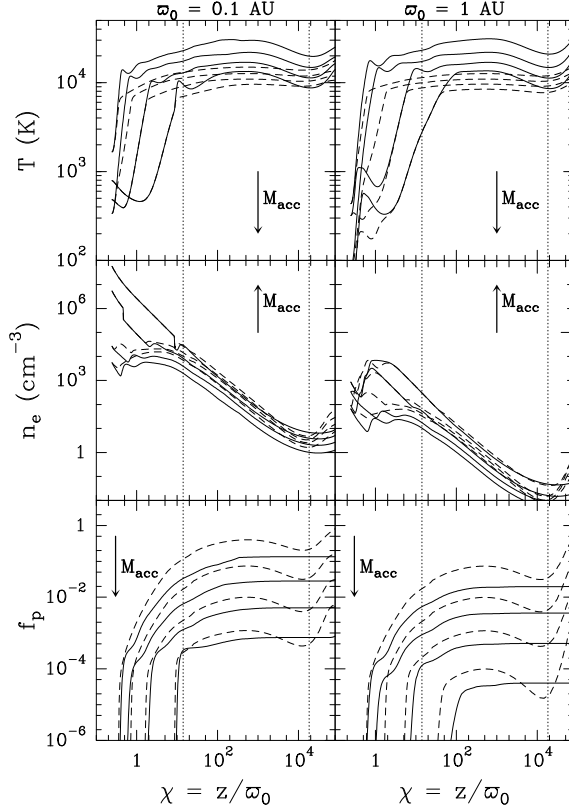


Fig. 1. Temperature T , electronic density n_e , and proton fraction $f_p = n(\text{H}^+)/n_{\text{H}}$ along two streamlines anchored at $\varpi_0 = 0.1$ AU (left column) and $\varpi_0 = 1$ AU (right column), for a disk wind with $\xi = 0.007$. For comparison, dashed curves show calculations with local ionization equilibrium imposed. \dot{M}_{acc} increases in the direction of the arrow from 10^{-8} and $10^{-5} M_{\odot} \text{ yr}^{-1}$ by factors of 10. Dotted vertical lines mark the locus of the Alfvén surface ($\chi \simeq 10$) and the point of maximum streamline opening ($\chi \simeq 2 \times 10^4$) before refocusing.

the temperature plateau, f_p is roughly inversely proportional to \dot{M}_{acc} and ϖ_0 .

- The electron density n_e is dominated by photoionization of heavy elements at the wind base, but is weakly dependent on \dot{M}_{acc} further out.

- The main heating process is ambipolar diffusion, Γ_{drag} , and the main cooling term is adiabatic expansion, Λ_{adia} . A close match between the two terms is established in the temperature plateau region (see Fig. 2).

Remarkably, the same behaviors were found for the solutions investigated by Safier (1993a). In the next section we explain why they are generic properties of self-similar cold MHD disk winds.

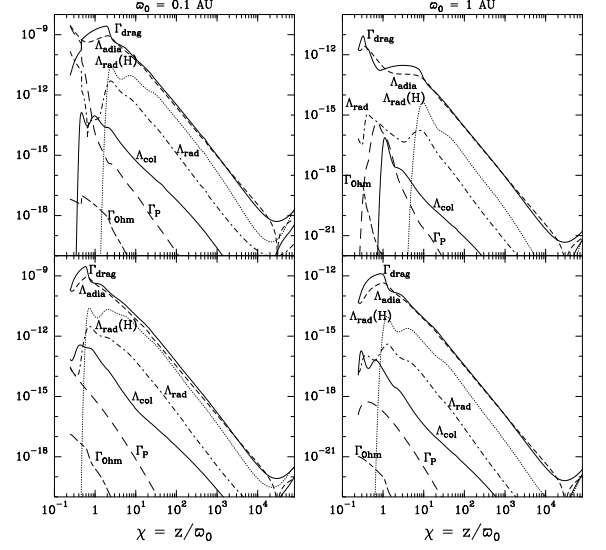


Fig. 2. Heating and cooling terms (in $\text{erg s}^{-1} \text{ cm}^{-3}$) for the same model as in Fig. 1. Top: $\dot{M}_{\text{acc}} = 10^{-6} M_{\odot} \text{ yr}^{-1}$, Bottom: $\dot{M}_{\text{acc}} = 10^{-7} M_{\odot} \text{ yr}^{-1}$.

2.4. Physical Origin of the Hot Temperature Plateau

It is useful to write the temperature evolution equation as a function of $\chi = z/\varpi_0$ as:

$$\begin{aligned} \frac{d \ln T}{d \ln \chi} &= -\frac{2}{3} \frac{d \ln \tilde{n}}{d \ln \chi} \times \left(\frac{\Gamma_{\text{drag}}}{\Lambda_{\text{adia}}} - 1 \right) \\ &= \delta^{-1} \times \left(\frac{G(\chi)}{F(T)} - 1 \right), \end{aligned} \quad (1)$$

where \tilde{n} is the wind particle density, δ is a positive function of order 1 before jet recollimation,

$$G(\chi) = -\frac{c^{-2} \|\vec{J} \times \vec{B}\|^2}{\tilde{n}^2 (\vec{v} \cdot \vec{\nabla}) \tilde{n}} \quad (2)$$

is another positive function (before recollimation) that depends only on the MHD wind solution, while

$$F(T) = kT (1 + f_e) m_{\text{in}} f_i f_n \langle \sigma_{\text{in}} v \rangle \times \left(\frac{\rho}{\rho_n} \right)^2 \quad (3)$$

depends only on the local temperature and ionization state of the gas.

One can see that $F(T)$ always increases as a function of temperature: either linearly $\propto T f_i$ when ionization is fixed (by photoionization or freeze-out), or much more steeply when collisional ionization of H is efficient, around 10^4 K. These two regimes of $F(T)$ are illustrated in Figure 3 in the case of local ionization equilibrium. The function $G(\chi)$ is also plotted in Fig. 3 for our solutions. It increases very rapidly

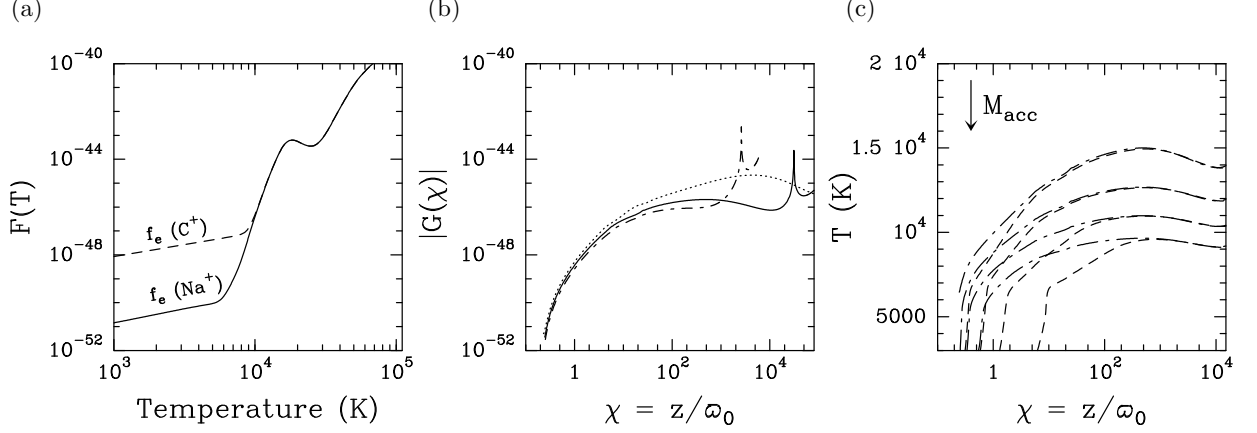


Fig. 3. (a) $F(T)$ in $\text{erg g cm}^3 \text{ s}^{-1}$ assuming local ionization equilibrium and photoionization of Na only (solid) or C (dashed). (b) $G(\chi)$ in $\text{erg g cm}^3 \text{ s}^{-1}$ for models A, B, C (bottom to top), $\omega_0 = 0.1 \text{ AU}$ and $\dot{M}_{\text{acc}} = 10^{-6} M_{\odot} \text{ yr}^{-1}$. (c) Temperature for model B assuming ionization equilibrium (dashed), compared with $T_c(\chi)$ as given by Eq. 4 (dot-dashed). $\omega_0 = 0.1 \text{ AU}$ and $\dot{M}_{\text{acc}} = 10^{-8}$ to $10^{-5} M_{\odot} \text{ yr}^{-1}$, from top to bottom.

at the base of the flow and then stabilizes in a plateau beyond the Alfvén point.

Now let us define a temperature $T_c(\chi)$ such that:

$$F(T_c) = G(\chi) \iff \Gamma_{\text{drag}} = \Lambda_{\text{adia}}. \quad (4)$$

Since F increases with temperature, it can be readily seen that if at a given point $T > T_c(\chi)$, then $G(\chi)/F(T) < 1$ and the gas will cool. Conversely, if $T < T_c(\chi)$, the gas will heat up. Thus, the fact that $F(T)$ is a rising function introduces a feedback that tries to bring the temperature near its local equilibrium value $T_c(\chi)$, and Λ_{adia} near Γ_{drag} .

However, $T \simeq T_c(\chi)$ is not necessarily a possible solution of equation (1): in that case the right-hand term is close to zero (by definition of T_c in Eq. 4) hence one must also have $d \ln T_c / d \ln \chi \ll 1$ for consistency: Only when $T_c(\chi)$ is flat can T converge to T_c , and can we have a temperature plateau with $\Lambda_{\text{adia}} \simeq \Gamma_{\text{drag}}$.

Indeed, T_c is, for our models, a flat function. We can understand this by differentiating Eq. 4:

$$\frac{d \ln G}{d \ln \chi} = \left(\frac{d \ln F}{d \ln T} \right)_{T=T_c} \left(\frac{d \ln T_c}{d \ln \chi} \right). \quad (5)$$

Hence $|d \ln T_c / d \ln \chi| \ll 1$ is equivalent to $|d \ln G / d \ln \chi| \ll |d \ln F / d \ln T|$. This is fulfilled for our models: Below the Alfvén surface, G varies a lot, but collisional H ionization is sufficiently close to ionization equilibrium that $F(T)$ still rises steeply around 10^4 K (cf. Fig. 3). For our numerical values of G , we have $T_c \simeq 10^4$ K and thus $|d \ln G / d \ln \chi| \ll |d \ln F / d \ln T|$. Further out, where ionization is frozen out, we have $d \ln F / d \ln T = 1$

(because $F \propto T f_i$) but it turns out that in this region G is a slowly varying function of χ , and thus we still have $|d \ln G / d \ln \chi| \ll |d \ln F / d \ln T|$.

The behavior of f_p when $G = F$ can also be understood: in self-similar disk wind models, G scales as $1/(\omega_0 \dot{M}_{\text{acc}})$. Since $F(T) \propto T f_p$ (when $f_e \ll 1$) and f_p is a high power of T close to ionization equilibrium, most of this scaling is absorbed by f_p , while T remains around 10^4 K for a wide range of model parameters. Note also that inclusion of thermal speeds (cf. Draine 1980) increases $\langle \sigma_{\text{in}} v \rangle$ by $\simeq 10$ compared to Safer (1993a) and decreases our values of f_p by the same amount, since only the product of these two terms enters in $F(T)$.

We conclude that MHD winds heated by ambipolar diffusion have a hot temperature plateau only when several conditions are met: (1) G must be such that $F = G$ happens around 10^4 K, (2) the wind must be in ionization equilibrium or near it in regions where G is a fast function of χ ; (3) once we have ionization freezing, G must vary slowly. For example, in the models of Ruden et al. (1990), ionization is quickly frozen while $G \propto 1/r$, hence no temperature plateau can be established (one has instead $T \propto 1/r$).

3. PREDICTED FORBIDDEN LINE EMISSION AND COMPARISON WITH OBSERVATIONS

We compute observational predictions assuming that the disk wind extends from 0.07 AU (typical disk corotation radius for a T Tauri star) to 1 AU. Inside corotation, the disk is expected to be truncated by the stellar magnetosphere, while beyond

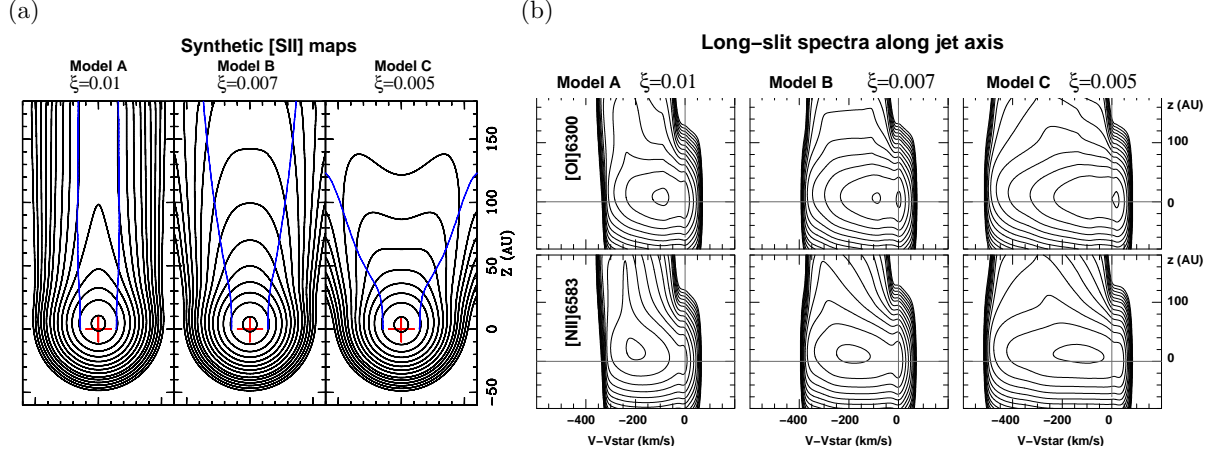


Fig. 4. (a) Emission maps and (b) long slit spectra along the jet axis for the all models and several forbidden lines. The inclination angle is $i = 60^\circ$ from pole-on, and mass accretion rate is $\dot{M}_{\text{acc}} = 10^{-6} M_\odot \text{ yr}^{-1}$. Intensity maps are convolved with a 28 AU resolution beam ($0.2''$ in Taurus) and long-slit spectra are convolved by $70 \text{ AU} \times 10 \text{ km s}^{-1}$, representative of current ground-based spectroimaging performances. Contours decrease by factors of 2.

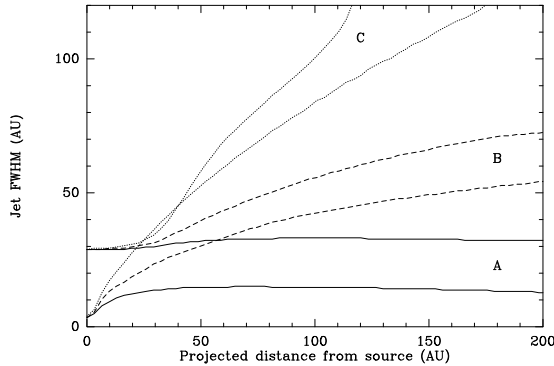


Fig. 5. Predicted jet transverse FWHM (obtained with Gaussian fits) for models A, B, C (with $\xi = 0.01, 0.007, 0.005$) and two different beam sizes: 28 AU and 2.8 AU corresponding in Taurus to $0.2''$ and $0.02''$ (VLT diffraction limit). Note the strong dependence on ξ and the bias introduced by the beam size.

1 AU, the wind should become molecular and not contribute to forbidden line emission (Safier 1993a).

Given the strong gradients in physical conditions present in the wind, care was taken to convolve synthetic maps and spectra to typical resolutions, to allow meaningful comparison with observations. The successes and failures of our model predictions are outlined below.

3.1. Wind Morphology: Emission Maps

The predicted maps for our models (Figure 4) successfully reproduce two features present in observed microjets: (1) an unresolved peak slightly

shifted from the stellar position, (2) jet-like emission appearing collimated within 200 AU of the star. Note that the MHD disk wind solutions considered by Safier 1993a did not collimate over such scales.

The shift of the unresolved peak cannot be used as model test because observed shifts are severely biased by accuracy of continuum subtraction (2% errors in subtraction imply ~ 4 AU error for bright jets Garcia, Thiébaut, & Bacon 1999) and by possible obscuration by a flared disk.

The jet FWHM, in contrast, provides an excellent quantitative test of the model: It is almost independent of the inclination angle, accretion rate and line, but is strongly dependent on the MHD dynamical solution (Figures 4, 5). Note that it is also severely biased by the beam size (Figure 5), an illustration of the importance of proper convolution before comparing to observations.

Predicted jet FWHM for models A and B ($\xi = 0.007-0.01$) agree very well with observations of T Tauri microjets at the same resolution (Dougados et al. 2000 and in this volume). Models with lower ξ (e.g., model C) are excluded. Note that at sufficiently high spatial resolution, disk jets should appear hollow, hence it would be important to get very high angular resolution data.

3.2. Wind Kinematics: Line Profiles

Typical long-slit spectra are presented in the right panels of Fig. 4, and integrated spectra for a wider range of parameters are plotted in Figure 6. The predictions are successful in several respects:

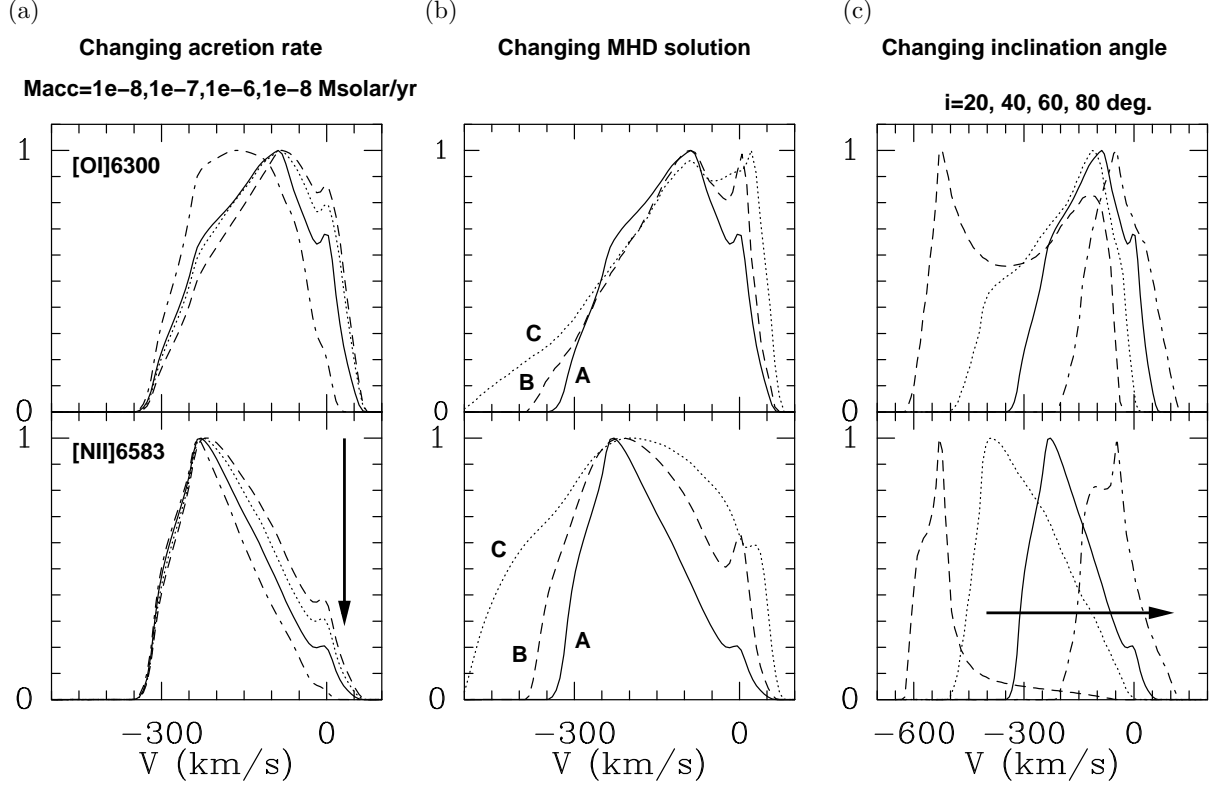


Fig. 6. Influence of model parameters on line profiles. (a) Effect of accretion rate. The arrow points in the direction of increasing \dot{M}_{acc} . (b) Effect of MHD solution. (c) Effect of inclination angle. The arrow points in the direction of increasing i .

(i) A compact low-velocity component (LVC) is produced near the star (Fig. 4), originating at the base of the slowly rotating outer disk streamlines. The LVC is stronger in [O I] than in [N II], and is stronger for low accretion rates (Fig. 6), as observed (HEG95).

(ii) An extended high-velocity component (HVC) is also present, tracing the accelerated regions of the wind. It is displaced further from the stellar position than the LVC, and the displacement is larger in [N II] than in [O I] (Fig. 4), as observed (Hirth et al. 1997). The [N II] line profile peaks at the blue edge of the [O I] line profile (Fig. 6), as also observed (HEG95).

However, we fail to reproduce some observed features:

(i) The relative intensity of the LVC with respect to the HVC is too small. At $i < 60^\circ$, it does not appear anymore as a distinct component in the [O I] profile. This weakness of the LVC stems from the low temperature and ionization below the Alfvén surface, where low-velocity gas is located.

(ii) Predicted centroid and maximum radial velocities of [O I] profiles agree well with observations of the DG Tau microjet, but are too high compared with typical TTS profiles (HEG95) unless most stars are observed at $i \geq 80^\circ$ (see Figure 6). Terminal velocities in cold disk wind models are $\simeq V_{\text{kep}}(\varpi_0)/\sqrt{\xi}$, so even our highest $\xi = 0.01$ (model A) gives excessive speeds.

3.3. Integrated Line Fluxes

Several trends are well reproduced: Predicted integrated fluxes increase linearly with accretion rate, as observed (HEG95). This is an interesting consequence of the weak dependence of n_e in the jet on \dot{M}_{acc} (cf. Fig. 1): emissivity ($\propto n_e n_H$) is then proportional to total density n_H , instead of n_H^2 as would be the case for a constant ionization fraction. We also find a correlation between integrated fluxes in [O I] and [S II], with a slope close to that observed (see Cabrit et al. 1990).

Quantitatively, however, integrated fluxes are systematically too weak compared to observations of TTS, for the same range of accretion rates, i.e.,

10^{-8} – $10^{-5} M_{\odot} \text{ yr}^{-1}$ (HEG95). We find $L([\text{O I}])$ in $L_{\odot} \simeq \dot{M}_{\text{acc}}$ in $M_{\odot} \text{ yr}^{-1}$. The discrepancy is typically a factor 30 for a given \dot{M}_{acc} . In the next section, we show that the flux deficit stems from insufficient n_e , but also possibly from insufficient total density n_H in our models.

3.4. Forbidden Line Ratios and Total Wind Densities

As noted by Bacciotti & Eisloffel (1999), forbidden line ratios of $[\text{S II}] 6716/6731$, $[\text{N II}]/[\text{O I}]$, and $[\text{S II}]/[\text{O I}]$ reflect directly the values of n_e , f_e , and T . Hence, they test mainly the heating mechanism, not the underlying dynamical solution.

Spatially resolved line ratios within 200 AU of the star are available for four TTS microjets: HH 30, Th 28, DG Tau, and RW Aur (Bacciotti & Eisloffel 1999; Lavalley-Fouquet et al. 2000; Bacciotti et al. and Dougados et al., this volume). Comparison with our predictions, *at the same beam resolution and distance from the star*, indicates that our models have slightly too high temperatures, and beam-averaged n_e and f_e that are too low by up to a factor 30. Two important remarks are in order:

(1) Because of volume effects and strong density gradients, beam-averaged line ratios differ greatly from local line ratios, and give very little weight to the inner densest parts of the wind. Hence it is essential to apply proper convolution to perform meaningful comparison with observed ratios.

(2) No ad-hoc heating rate tuning is present in our model. Predicted line ratios would improve if we include extra mechanical energy deposition, e.g., in shocks, as illustrated in Dougados et al. (this volume), or with a dissipation length prescription, as done in Shang et al. (this volume).

For the latter reason, the total density $n_H = n_e/f_e$ is a more useful quantity that can be directly compared with model predictions independently of the ionization process (although it can still be affected by shock compression and by beam averaging). For accretion rates of $10^{-6} M_{\odot} \text{ yr}^{-1}$, total densities on the innermost streamline for our models are too low by a factor 10–100 compared to observations of the above four bright T Tauri microjets. Shock compression could explain a factor of 10 (Hartigan et al. 1994), but it seems that our models have intrinsically too low density close to the star.

4. CONCLUDING REMARKS

We extended the original work of Safier (1993a,b), and compute the thermal structure of a disk wind jet, assuming current dissipation in

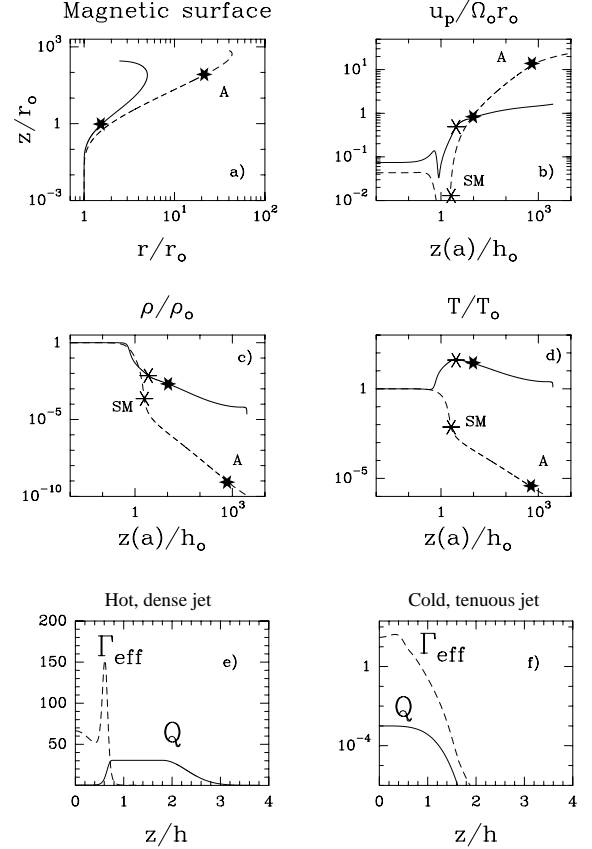


Fig. 7. Upper 4 panels: New MHD disk wind solutions with large heating at the disk surface (solid curves) have: more collimated streamlines (top left), lower terminal velocity (top right), and higher density (middle left) than a model with small heating (dashed curves). Bottom panels: Local energy dissipation rate (Joule and viscous; Γ_{eff}), and prescribed entropy injection Q for the 2 models displayed above. See Casse & Ferreira (2000) for details.

ion-neutral collisions—ambipolar diffusion—as the major heating source. Improvements include: (a) detailed dynamical models where the disk is self-consistently taken into account; (b) ionization evolution for all relevant “heavy atoms”; (c) radiation cooling by hydrogen lines, recombination and photoionization heating; (d) correct H-H⁺ momentum exchange rates; and (e) more detailed dust description. We still obtain warm jets 10⁴ K but with ionizations fractions 10 to 100 times smaller than Safier, due to larger H-H⁺ momentum exchange rates (including the dominant thermal velocity contribution) and to different MHD wind dynamics.

We have presented a complete set of predictions for forbidden line emission, where we have stressed

the crucial effect of beam convolution. The model reproduces several observed trends: (1) images show an unresolved peak and an extended high-velocity jet, of width compatible with observations. (2) Line profiles present a low-velocity component (LVC), compact and near the star, and a high-velocity component (HVC), tracing the jet. The systematic differences between [O I] and [N II] profiles are reproduced. (3) Line fluxes are proportional to \dot{M}_{acc} , and the [O I]-[S II] correlation slope is recovered.

Other line ratios ([S II] 6716/6731, [N II]/[O I]) are not well reproduced, but we stress that they trace only the excitation conditions, which depend mainly on the heating mechanism, and do not test the underlying dynamical model; a better fit could be readily obtained with an extra tunable heating rate, such as done e.g., by Shang et al. (this volume) or with shocks (Dougados et al., this volume).

Two intrinsic properties of our dynamical models are not fully successful: Wind terminal velocities appear too high, and densities at the wind base appear too small, when compared with current estimates in bright microjets. One possible improvement would be to relax the assumption of a cold disk wind, and include heating at the disk surface (Casse & Ferreira 2000). MHD disk winds with higher density and lower terminal velocities can then be obtained (see Figure 7). The self-consistent thermal structure of these solutions remains to be investigated.

REFERENCES

- Bacciotti, F., Eisloffel, J. 1999, A&A, 342, 717
 Bacciotti, F. 2002, RevMexAA(SC), 13, 8 (this volume)
 Binette, L., et al. 1985, ApJ, 297, 476
 Binette, L. & Robinson, A. 1987, A&A, 177, 11
 Blandford, R. D., & Payne, D. G. 1982, MNRAS, 199, 883
 Burrows, C. J., et al. 1996, ApJ, 473, 437
 Cabrit, S., et al. 1990, ApJ 354, 687
 ———. 1999, A&A 343, L61
 Casse, F., & Ferreira, J. 2000, A&A 361, 1178
 Cohen, M., et al. 1989 ApJ, 339, 455
 Dougados, C., Cabrit, S., & Lavalley-Fouquet, C. 2000, A&A 357, L61
 ———. 2002, RevMexAA(SC), 13, 43 (this volume)
 Draine, B. T. 1980, ApJ, 241, 1021
 Ferreira, J. 1997, A&A, 319, 340
 Garcia, P. J. V., Thiébaud, E., & Bacon, R. 1999, A&A, 346, 892
 Garcia, P. J. V., Cabrit, S., Ferreira, J., & Binette, L. 2001a, A&A, 377, 609
 Garcia, P. J. V., Ferreira, J., Cabrit, S., & Binette, L. 2001b, A&A, 377, 589
 Hartigan, P., Morse, J., & Raymond, J. 1994, ApJ 436, 125
 Hartigan, P., et al. 1995, ApJ 452, 736 (HEG95)
 Hirth, G. A., et al. 1994, ApJ, 427, L99
 ———. 1997, A&ASS, 126, 437
 Kwan, J. 1997, ApJ, 489, 284
 Kwan, J., & Tademaru, E. 1988, ApJ, 332, L41
 ———. 1995, ApJ, 454, 382
 Lavalley-Fouquet, C., et al. 2000, A&A 356, L41
 Ray, T., & Mundt, R. 2002, RevMexAA(SC), 13, 83 (this volume)
 Ruden, S. P., et al. 1990, ApJ, 361, 546
 Safier, P. N. 1993a, ApJ, 408, 115
 ———. 1993b, ApJ, 408, 148
 Savage, B. D., & Sembach, K. R. 1996, ARA&A, 34, 279
 Shang, H., Shu, F., & Glassgold, A. 1998, ApJ 493, L91
 Shu, F., et al. 1995, ApJ 455, L155

- P. Garcia: Centro de Astrofísica da Univ. Porto, Rua das Estrelas s/n, 4150-762 Porto, Portugal (pgarcia@astro.up.pt).
 S. Cabrit: DEMIRM, Observatoire de Paris, 61 Avenue de l'Observatoire, F-75014 Paris (sylvie.cabrit@obspm.fr).
 J. Ferreira and F. Casse: LAOG, Observatoire de Grenoble, BP 53, F-38041 Grenoble Cedex 9 (ferreira@obs.ujf-grenoble.fr).
 L. Binette: Instituto de Astronomía, UNAM, Apartado Postal 70-264, 04510 México, D. F. (binette@astroscu.unam.mx)